

Polarization of Thermal Dilepton Radiation

Florian Seck,¹ Bengt Friman,^{2,1} Tetyana Galatyuk,^{2,1} Hendrik van Hees,^{3,4} Enrico Speranza,⁵ Ralf Rapp,⁶ and Jochen Wambach¹

¹*Technische Universität Darmstadt, 64289 Darmstadt, Germany*

²*GSI Helmholtzzentrum für Schwerionenforschung GmbH, 64291 Darmstadt, Germany*

³*Institut für Theoretische Physik, Goethe-Universität Frankfurt am Main, Max-von-Laue-Strasse 1, D-60438 Frankfurt am Main, Germany*

⁴*Helmholtz Research Academy Hesse for FAIR, Campus Frankfurt, 60438 Frankfurt, Germany*

⁵*University of Illinois at Urbana-Champaign, Urbana, IL 61801, USA*

⁶*Texas A&M University, College Station, TX 77843-3366, USA*

(Dated: September 7, 2023)

The spectra of dileptons radiated from the fireballs formed in high-energy heavy-ion collisions have been successfully used to investigate key properties of hot and dense QCD matter. In this paper we study polarization observables which have thus far received little attention. Microscopic calculations of in-medium electromagnetic spectral functions have thus far mostly focused on integrated yields which are proportional to the sum of the longitudinal and transverse components of the virtual photon's selfenergy. Photon polarization results from the difference of these components, which in general does not vanish for lepton pairs at finite three-momentum relative to the heat bath (and is maximal for fully transverse real photons). Using a model that successfully describes dilepton spectra in heavy-ion collisions, with hadronic emission via medium-modified vector mesons and quark-antiquark annihilation constrained by lattice QCD, we compute polarization observables in different dilepton mass bins and confront them with data of the HADES and NA60 experiments.

Measurements of electromagnetic (EM) radiation from high-energy heavy-ion collisions have provided unprecedented insights into the properties of Quantum Chromodynamics (QCD) matter formed in these reactions. Over the last decade, a rather consistent picture has emerged in interpreting the observed dilepton spectra. At low invariant masses, commonly referring to $M \lesssim 1$ GeV, thermal radiation mostly emanates from the hadronic medium of the fireball evolution, with a strongly broadened ρ -meson peak indicating an ultimate melting and transition into a continuum of partonic degrees of freedom [1, 2]. Similar findings have also been reported at the higher energies of the Relativistic Heavy-Ion Collider (RHIC) [3] and the lower energies at the Schwerionensynchrotron (SIS18) [4]. On the other hand, in the intermediate-mass region (IMR), $1 \text{ GeV} \lesssim M \lesssim 3 \text{ GeV}$, the radiation contribution is strongly favored toward early phases, which, at least for collision energies of $\sqrt{s} \gtrsim 10 \text{ GeV}$, has been associated with partonic radiation sources [5], with temperatures well above the pseudocritical one obtained from lattice QCD, $T_{\text{pc}} \simeq 155\text{--}160 \text{ MeV}$ [6, 7]. Pertinent transverse-momentum (p_T) spectra corroborate these findings: The NA60 collaboration established that the well-known blue-shift effect due to a collectively expanding source is much less pronounced in the IMR compared to the low-mass region (LMR), implying earlier emission for the former compared to the latter.

Successful model descriptions of dilepton data have largely relied on hadronic many-body theory, where the predicted melting of the ρ -meson rather seamlessly transits into a structureless quark-antiquark continuum [8], albeit with substantial enhancements over the free $q\bar{q}$ rate

toward low masses. However, the precise micro-physics underlying the strongly coupled QCD liquid in the transition regime remains a matter of debate. Therefore, further tests of the existing model calculations would be very valuable. In this letter we demonstrate this in a first quantitative application to spin-polarization observables of low-mass dileptons in heavy-ion experiments.

The key quantity in our study is the EM emissivity of thermal QCD matter which is determined by the correlator of the EM current, schematically written as a thermal expectation value, $\Pi_{\text{EM}}^{\mu\nu} = \langle j_{\text{EM}}^\mu j_{\text{EM}}^\nu \rangle_T$, which can also be interpreted as the in-medium photon selfenergy. The pertinent spectral function, $\varrho_{\text{EM}}^{\mu\nu} = -2\text{Im}\Pi_{\text{EM}}^{\mu\nu}$, figures in the dilepton emission rate as

$$\frac{dN_{ll}}{d^4x d^4q} = \frac{\alpha^2 L(M)}{6\pi^3 M^2} f^B(q_0; T) g_{\mu\nu} \varrho_{\text{EM}}^{\mu\nu}(M, |\vec{q}|; T, \mu_B) \quad (1)$$

where $M = \sqrt{q_0^2 - \vec{q}^2}$ denotes the dilepton invariant mass, $f^B(q_0; T) = 1/(e^{q_0/T} - 1)$ the thermal Bose function, $\alpha \simeq 1/137$ the fine-structure constant and $L(M)$ a lepton phase-space factor ($L(M)=1$ for lepton masses $m_l \ll M$). Using the standard 4D projectors for a spin-1 particle, $P_{L,T}^{\mu\nu}$, one can decompose the spectral function into its longitudinal and transverse components as [9, 10]

$$\varrho_{\text{EM}}^{\mu\nu} = \varrho_L P_L^{\mu\nu} + \varrho_T P_T^{\mu\nu}, \quad (2)$$

rendering $g_{\mu\nu} \varrho_{\text{EM}}^{\mu\nu} = \varrho_L + 2\varrho_T$. At vanishing 3-momentum in the heat bath one has $\varrho_T = \varrho_L$, but at finite $|\vec{q}|$ this no longer holds as spherical symmetry is broken.

Angular dependencies in the dilepton production rate can be unravelled by resolving the angle, $\Omega_l = (\phi_l, \theta_l)$,

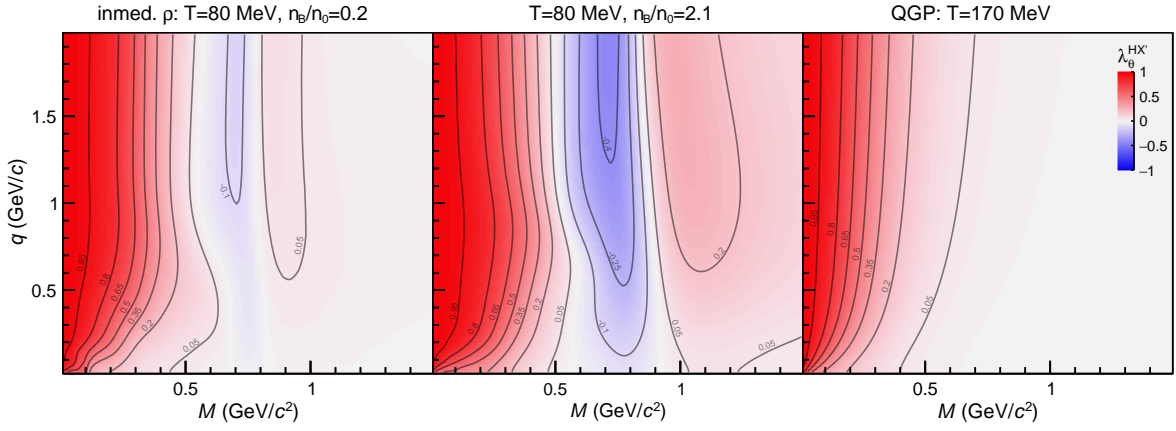


FIG. 1. Anisotropy coefficient, $\lambda_\theta^{HX'}$ from Eq. (6), for EM spectral functions in static hadronic matter at $T=80$ MeV and baryon densities $n_B=0.2 n_0$ (left panel) and $n_B=2.1 n_0$ (middle panel), and in a static QGP at $T=170$ MeV (right panel).

of a single lepton relative to the photon's momentum in the latter's rest frame [11–13]. It can be shown that

$$\frac{dN_{ll}}{d^4x d^4q d\Omega_l} = \frac{\alpha^2}{32\pi^4} \frac{1}{M^4} \sqrt{1 - \frac{4m_l^2}{M^2}} \varrho_{EM}^{\mu\nu} L_{\mu\nu} f^B(q_0; T), \quad (3)$$

with the lepton tensor

$$L^{\mu\nu} = 2(q^2 g^{\mu\nu} - q^\mu q^\nu + \Delta l^\mu \Delta l^\nu), \quad (4)$$

where $\Delta l^\mu = l^{+\mu} - l^{-\mu}$, and l^\pm are the lepton 4-momenta. More explicitly, the angular distribution takes the form

$$\begin{aligned} \frac{dN_{ll}}{d^4x d^4q d\Omega_l} \propto & \left(1 + \lambda_\theta \cos^2 \theta_l \right. \\ & + \lambda_\phi \sin^2 \theta_l \cos 2\phi_l + \lambda_{\theta\phi} \sin 2\theta_l \cos \phi_l \\ & \left. + \lambda_\phi^\perp \sin^2 \theta_l \sin 2\phi_l + \lambda_{\theta\phi}^\perp \sin 2\theta_l \sin \phi_l \right), \end{aligned} \quad (5)$$

where the λ 's are the anisotropy coefficients.

Well-known examples in this context are the Drell-Yan process (leading to predominately transverse polarization due to the collinear annihilation of the incoming quark and antiquark) and the high- p_T J/ψ polarization puzzle (where gluon fragmentation suggests transverse polarization which is at variance with experiment). Even in an isotropic thermal medium, nontrivial anisotropies in the angular distribution of the produced leptons occur, *e.g.*, for basic hadronic and partonic sources ($\pi\pi$ vs. $q\bar{q}$ annihilation, respectively) at a few percent level [13]. However, the effects are expected to become much larger toward smaller M , where more intricate production processes, such as resonance Dalitz decays or Bremsstrahlung occur and eventually lead to fully transverse polarization at the photon point ($M=0$). In addition, the anisotropy of lepton pairs in the $M=1$ -1.5 GeV region might be able to distinguish whether the so-called "chiral mixing" between ρ and a_1 channels via πa_1 annihilation or $q\bar{q}$ annihilation is the dominant source.

For the present study we employ in-medium spectral functions that have been used enabling a fair description of available dilepton data from ultra-/relativistic heavy-ion collisions. It consists of hadronic emission with in-medium vector-meson spectral functions (mostly ρ -meson) calculated from hadronic many-body theory based on effective lagrangians [8, 14], supplemented with continuum-like multi-meson annihilation channels relevant at masses above ~ 1 GeV [15], and QGP emission based on perturbative $q\bar{q}$ annihilation with a low-energy transport peak constrained by IQCD data [16]. The transitioned from hadronic to QGP radiation is carried out at a temperature of 170 MeV, where the two rates are close to each other.

Let us start by inspecting the pertinent anisotropy coefficient in a static thermal medium, characterized by a 4-velocity $u = \gamma(1, \vec{\beta}) = (1, 0, 0, 0)$, where the rotational symmetry is only broken by the virtual photon's momentum direction. Taking the polarization axis as z' in the helicity frame HX' the anisotropy coefficient λ_θ is given by

$$\lambda_\theta^{HX'}(M, |\vec{q}|) = \frac{\varrho_T - \varrho_L}{\varrho_T + \varrho_L}, \quad (6)$$

which highlights its dependence on the *difference* between the polarization component of the EM spectral function; the pertinent results for hadronic matter and QGP are displayed in Fig. 1. All other anisotropy coefficients are zero as they involve asymmetries with respect to the ϕ_l angle of the leptons. The hadronic spectral function exhibits a strong dependence of λ_θ , in particular on baryon density and, nonmonotonously, on invariant mass, while QGP emission is rather little polarized except when approaching the photon point, for $M \lesssim 0.5$ GeV.

To evaluate dilepton radiation in a heavy-ion collision one usually divides the expanding fireball into small cells of locally thermalized matter with velocity $u = \gamma(1, \vec{\beta})$ in the center-of-mass frame of the collision (as is rou-

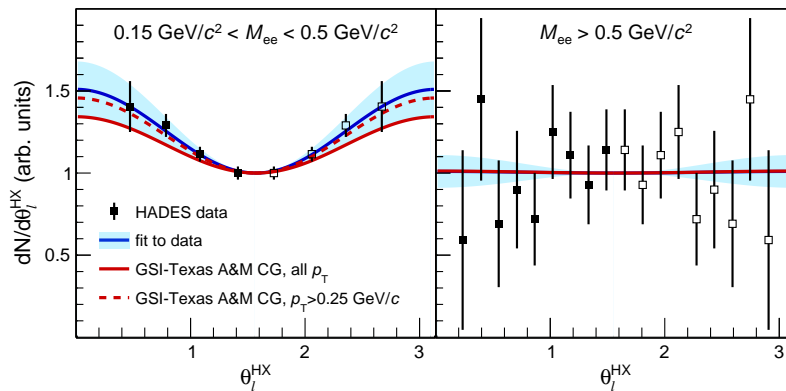


FIG. 2. Comparison of calculated angular distributions (red lines), integrated over 2 dielectron mass bins, to HADES data in Ar(1.76 GeV)+KCl collisions [4]. Fits by the HADES collaboration (blue lines with bands) yield anisotropy parameters of $\lambda_\theta = 0.51 \pm 0.17$ (left panel) and 0.01 ± 0.1 (right panel) for the lower and higher mass window, respectively, compared to 0.34 and 0.01 from the calculations. To illustrate effects of a finite HADES acceptance, we also show theoretical results with a cut on transverse pair momentum in the lab of $p_T > 0.25$ GeV (dashed red line).

tinely done in hydrodynamic simulations). To compute the polarization of a lepton pair within each cell, the local helicity frame HX' can be reached by a boost into the rest frame of the virtual photon. The task is now to transform the local polarization from the HX' frame, where only $\lambda_\theta^{\text{HX}'}$ is finite, into a global frame that is accessible to experiments. Common choices are the helicity frame (HX) or the Collins-Soper frame (CS), where some (or all) anisotropy coefficients can acquire non-zero values.

We start from the virtual photon with (observed) 4-momentum $p^\mu = (p_0, 0, 0, p)$ in the center-of-mass system (CMS) of the collision, defining the z -axis along its 3-momentum, \vec{p} . In the helicity frame (HX) this defines the polarization axis while the pertinent y -axis is defined by the normal vector of the plane spanned by the beam momenta, and thus defines the (xyz) system. On the other hand, the z' axis is defined in the thermal rest frame, which is moving with the medium's flow velocity u^μ in the CMS. The photon 4-momentum in this system, q^μ , is obtained from the Lorentz boost of p^μ using u^μ , and determines the only finite coefficient in this system, $\lambda_\theta^{\text{HX}'}$. With the above definitions, one can then transform the angular distribution into the HX system by a succession of 3 Euler rotations:

- (i) around the z' -axis by an angle ψ to bring the y -axis perpendicular to the z -axis;
- (ii) around the thus obtained y'' axis by an angle ζ to align the z' -axis with the z -axis; and
- (iii) around the z -axis by an angle ω to align the x' - and y' -axes along the x - and y -axes, respectively.

In this way, all five coefficients in Eq. (5) can be determined from $\lambda_\theta^{\text{HX}'}$ and the three rotation angles described above. A similar procedure can be carried when measuring the polarization in the Collins-Soper frame, which will be detailed elsewhere.

To compare to experiment, the contributions to the

anisotropy coefficients in given frame (*e.g.*, HX) from all medium cells need to be accounted for. In practice this is achieved via a yield-weighted mean,

$$\lambda_\theta^{\text{HX}}(M, p_T, y, \phi) = \frac{\sum_{\text{all cells}} \mathcal{N}_{\text{cell}} \lambda_{\theta, \text{cell}}^{\text{HX}}}{\sum_{\text{all cells}} \mathcal{N}_{\text{cell}}} = \frac{\sum_{\text{all cells}} \mathcal{N}_{\text{cell}} \lambda_{\theta, \text{cell}}^{\text{HX}}}{\mathcal{N}_{\text{fireball}}} \quad (7)$$

with a cell weight

$$\mathcal{N}_{\text{cell}} = \frac{dN_{\text{cell}}}{dM dp_T dy d\phi} = \frac{dR(T_{\text{cell}}, \mu_{B, \text{cell}})}{dM dp_T dy d\phi} \times V_{\text{cell}} t_{\text{cell}} \quad (8)$$

where V_{cell} denotes the cell's 3-volume and t_{cell} the time discretization interval, and

$$\frac{dR}{dM dp_T dy d\phi} = M p_T \frac{dR}{d^4q} \quad (9)$$

(note that dR/d^4q is Lorentz-invariant). As needed, kinematic variables can be integrated over (especially due to limited statistics in experiment), *e.g.*, for the anisotropy coefficient, $\lambda_\theta^{\text{HX}}(M)$, as a function of invariant mass as

$$\begin{aligned} \lambda_\theta^{\text{HX}}(M) &= \frac{\int \mathcal{N}_{\text{fireball}} \lambda_\theta^{\text{HX}}(M, p_T, y, \phi) dp_T dy d\phi}{\int \mathcal{N}_{\text{fireball}} dp_T dy d\phi} \\ &= \frac{\sum \mathcal{N}_{\text{fireball}} \lambda_\theta^{\text{HX}}(M, p_T, y, \phi) \Delta p_T \Delta y \Delta \phi}{\sum \mathcal{N}_{\text{fireball}} \Delta p_T \Delta y \delta \phi} \end{aligned} \quad (10)$$

where Δp_T , Δy , and $\Delta \phi$ are the bin widths for transverse momentum, rapidity, and azimuthal angle, respectively.

We first compare our results to HADES data [4] measured in Ar(1.76 AGeV)+KCl collisions, cf. Fig 2. For this collision system, the discretization into space-time cells follows our previous work [18] employing a coarse-graining of the UrQMD transport model, without the

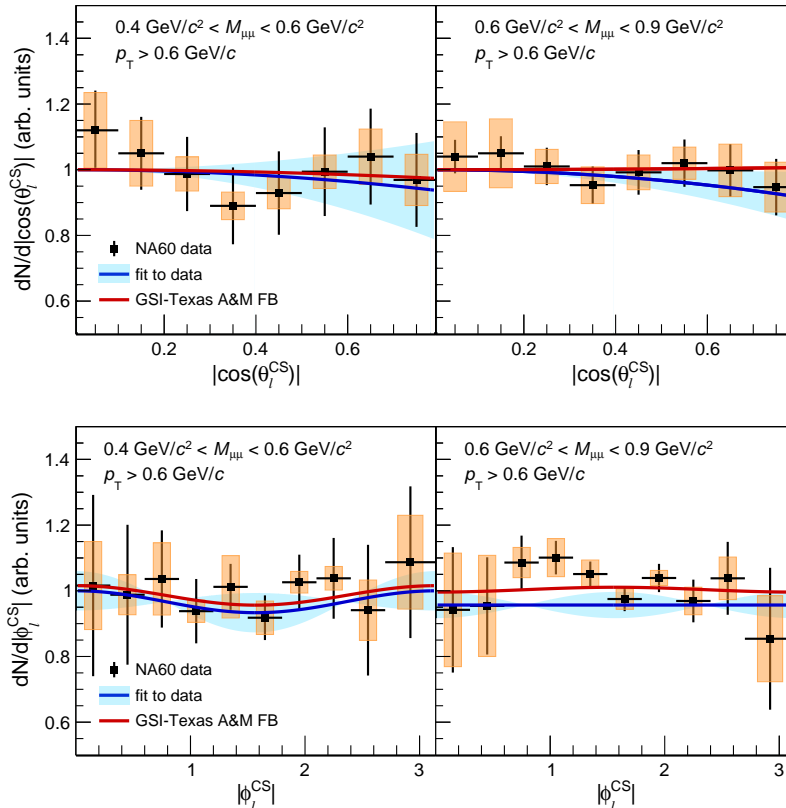


FIG. 3. Calculated angular distributions (red lines), integrated over two diuon mass windows, in the CS frame, compared to NA60 data in In(158 AGeV)+In collisions [17]. The blue lines represent fits by NA60 with extracted anisotropy parameters of $\lambda_\theta = -0.10 \pm 0.24$ (upper left) and -0.13 ± 0.12 (upper right), compared to the calculated values of -0.04 and 0.01 , respectively, and likewise $\lambda_\phi = 0.05 \pm 0.09$ (lower left) and 0.00 ± 0.06 (lower right), compared to 0.04 and -0.01 from our calculation.

formation of QGP phase. For both invariant mass bins shown in the 2 panels, the theoretical predictions (red lines) are in fair agreement with the data and are not far from functional best fit (blue lines). It turns out that the anisotropy coefficient λ_θ largely survives the transformations induced by the expansion of the medium (after all, the collective flow developed in Ar(1.76 AGeV)+KCl collisions is rather small). As such, the data directly reflect the polarization properties of the ρ spectral function shown in Fig. 1, which exhibits a transition from a predominantly transverse polarization for masses below 0.5 GeV (red region) to the regime where the (average) polarization is small.

Next, we turn to NA60 diuon data [17] from In(158 AGeV)+In collisions. For this system, we utilize the isentropically expanding fireball model whose particle content reproduces the experimentally observed light-hadron data and whose time evolution was constrained by observed p_T spectra and hydrodynamic expansion time scales [5, 15]. This model includes a QGP phase that reaches maximal initial temperatures of close to $T_0 = 240$ MeV. Also here, the theoretical predictions (in this case for the Collins-Soper frame) describe the

angular distributions in the ϕ_l and θ_l polarization angles quite well. Note, however, that the near absence of a net polarization (*i.e.*, the rather flat angular distributions) is not related to thermal isotropy arguments but due to the thermal properties of the EM spectral function used in this calculation, *i.e.*, the rather small net polarization of the in-medium ρ meson and of the QGP radiation in the mass region around ~ 0.5 GeV (recall Fig. 1).

In summary, we have extracted polarization properties of virtual photons from electromagnetic spectral functions of QCD matter that enable fair descriptions of existing data for mass and momentum spectra. While the latter rely on the sum of transverse and longitudinal components of the spectral function, polarization observables are sensitive to their difference. We find that thermal dileptons from dense hadronic matter exhibit a structure where transverse polarization at low masses transits into longitudinal one in the ρ -meson mass region. At high temperatures and smaller baryon densities these structures become less pronounced and more closely resemble QGP emission. We have applied these results to experimental observables, by carrying out the transformations from the thermal frame into angular variables observ-

able in the lab frame. Our predictions agree with both HADES and NA60 data fairly well, supporting the microscopic description underlying our model. In the future, we expect polarization observables to play an increasingly important role in exploring the mechanisms underlying EM emission spectra in heavy-ion collisions. Multi-differential measurements of the virtual photon polarization will become available from HADES, STAR and ALICE, as well as the future high-rate experiments CBM, NA60+ and ALICE3.

This work was supported by the Deutsche Forschungsgemeinschaft (DFG) through the grant CRC-TR 211 “Strong-interaction matter under extreme conditions”, by the U.S. National Science Foundation (NSF) under grant no. PHY-2209335 and the ExtreMe Matter Institute (RR).

-
- [1] G. Agakichiev et al. (CERES), *Eur. Phys. J. C* **41**, 475 (2005), [arXiv:nucl-ex/0506002](#).
 - [2] R. Arnaldi et al. (NA60), *Phys. Rev. Lett.* **96**, 162302 (2006), [arXiv:nucl-ex/0605007](#).
 - [3] L. Adamczyk et al. (STAR), *Phys. Rev. Lett.* **113**, 022301 (2014), [Addendum: *Phys.Rev.Lett.* 113, 049903 (2014)], [arXiv:1312.7397 \[hep-ex\]](#).
 - [4] G. Agakishiev et al. (HADES), *Phys. Rev. C* **84**, 014902 (2011), [arXiv:1103.0876 \[nucl-ex\]](#).
 - [5] R. Rapp and H. van Hees, *Phys. Lett. B* **753**, 586 (2016), [arXiv:1411.4612 \[hep-ph\]](#).
 - [6] A. Bazavov et al. (HotQCD), *Phys. Lett. B* **795**, 15 (2019), [arXiv:1812.08235 \[hep-lat\]](#).
 - [7] S. Borsanyi, Z. Fodor, J. N. Guenther, R. Kara, S. D. Katz, P. Parotto, A. Pasztor, C. Ratti, and K. K. Szabo, *Phys. Rev. Lett.* **125**, 052001 (2020), [arXiv:2002.02821 \[hep-lat\]](#).
 - [8] R. Rapp and J. Wambach, *Eur. Phys. J. A* **6**, 415 (1999), [arXiv:hep-ph/9907502](#).
 - [9] L. D. McLerran and T. Toimela, *Phys. Rev. D* **31**, 545 (1985).
 - [10] N. P. Landsman and C. G. van Weert, *Phys. Rept.* **145**, 141 (1987).
 - [11] E. L. Bratkovskaya, O. V. Teryaev, and V. D. Toneev, *Phys. Lett. B* **348**, 283 (1995).
 - [12] G. Baym, T. Hatsuda, and M. Strickland, *Phys. Rev. C* **95**, 044907 (2017), [arXiv:1702.05906 \[nucl-th\]](#).
 - [13] E. Speranza, A. Jaiswal, and B. Friman, *Phys. Lett. B* **782**, 395 (2018), [arXiv:1802.02479 \[hep-ph\]](#).
 - [14] R. Rapp, G. Chanfray, and J. Wambach, *Nucl. Phys. A* **617**, 472 (1997), [arXiv:hep-ph/9702210](#).
 - [15] H. van Hees and R. Rapp, *Nucl. Phys. A* **806**, 339 (2008), [arXiv:0711.3444 \[hep-ph\]](#).
 - [16] R. Rapp, *Adv. High Energy Phys.* **2013**, 148253 (2013), [arXiv:1304.2309 \[hep-ph\]](#).
 - [17] R. Arnaldi et al. (NA60), *Phys. Rev. Lett.* **102**, 222301 (2009), [arXiv:0812.3100 \[nucl-ex\]](#).
 - [18] T. Galatyuk, P. M. Hohler, R. Rapp, F. Seck, and J. Stroth, *Eur. Phys. J. A* **52**, 131 (2016), [arXiv:1512.08688 \[nucl-th\]](#).